

Kim Hyo-Im (Orcid ID: 0000-0001-5667-0060)

Lee Sung Keun (Orcid ID: 0000-0002-3149-3421)

Structural Transitions in MgSiO₃ Glasses and Melts at the Core-Mantle Boundary Observed *via* Inelastic X-ray Scattering

Yong-Hyun Kim¹, Yoo Soo Yi¹, Hyo-Im Kim¹, Paul Chow², Yuming Xiao², Guoyin Shen², Sung Keun Lee^{1,3*}

¹*School of Earth and Environmental Sciences, Seoul National University, 08826 Seoul, Korea*

²*HPCAT, X-ray Science Division, Argonne National Laboratory, Argonne, IL 60439, USA*

³*Institute of Applied Physics, Seoul National University, 08826 Seoul, Korea*

*correspondence Email: sungklee@snu.ac.kr (<http://hosting03.snu.ac.kr/~sungklee>)

Key points

- The O *K*-edge inelastic X-ray scattering spectra of MgSiO₃ glass up to 130 GPa revealed the bonding transitions around oxygen at CMB.
- The emergence of dense oxygen networks near megabar pressure stems from contractions in the Mg-O and O-O distances, unique to MgSiO₃ melts.
- The results provide insights into densification mechanism of dense partial melts anticipated to comprise the ULVZ at the CMB.

Abstract The structural adaptation in MgSiO₃ melts under compression up to 130 GPa is the key to revealing the origins of the pronounced negative buoyancy of the melts at the core-mantle boundary (CMB). A full understanding of the melt densification requires study of the pressure-induced changes in the bonding configuration around oxygen at the CMB, which has proven to be difficult to measure. Here, the experimental breakthrough in O *K*-edge inelastic X-ray scattering enables collection of the spectra of MgSiO₃ glasses up to ~130 GPa, along with *ab initio* molecular dynamics simulations, revealing the electronic bonding transitions around heavily compressed oxygen. The spectral results indicate the emergence of denser network structures around oxygen, stemming from contractions in the Mg-O and O-O distances associated with flexible topological and short-range rearrangements around Si. The results unveil the electronic structure and thus the nature of densification in dense partial melts at the CMB.

Plain language summary A thin ultralow-velocity zone (ULVZ) at the bottom of mantle is characterized by reduced seismic wave velocities and enhanced density, suggesting the possible presence of molten silicates at a depth of ~2850 km (~130 GPa of pressure). How the melts densify near the core-mantle boundary is unclear. Because oxygen occupies the

This article has been accepted for publication and undergone full peer review but has not been through the copyediting, typesetting, pagination and proofreading process which may lead to differences between this version and the Version of Record. Please cite this article as doi: 10.1029/2019GL085889

major volume fraction of silicates, the melt densification is dominated by the reorganization of oxygen during compression. However, the oxygen bonding environments in MgSiO_3 melt – a model mantle melt - near the CMB are unknown. Here, the inelastic X-ray scattering spectra of MgSiO_3 glasses and liquids up to ~ 130 GPa revealed the electronic bonding transitions around compressed oxygen that are not observed at low pressures and substantially differ from those in the crystalline MgSiO_3 bridgmanite. The spectral results indicate the pressure-induced emergence of denser network structures around oxygen, stemming from gradual contractions in the Mg-O and O-O distances associated with flexible topological and short-range rearrangements around Si. The densification around oxygen near megabar pressures potentially contributes to the gravitational stabilization of the complex partial melts in the deeper part of the mantle toward ULVZ.

1. Introduction

The presence of dense melts has been proposed to account for the ultralow-velocity zone (ULVZ) near the core-mantle boundary (CMB) at a depth of ~ 2850 km (~ 130 GPa) (Rost et al., 2005; Williams & Garnero, 1996), implying that the melts could be denser than silicate crystals near the bottom of the mantle, while the dense melts are seismically weak. The origins of the negative buoyancy of the melts and the stable presence of melts at the CMB are among the remaining puzzles in mineral physics. Furthermore, a large portion of bulk silicate Earth was once molten, forming a magma ocean toward the bottom of the primitive mantle during the Hadean phase. Density contrast between silicate crystals and melts has controlled whether the partial melts at the CMB may float or reside, which affected evolution of the magma ocean (Agee, 1998; Agee & Walker, 1988; Caracas et al., 2019; Labrosse et al., 2007; Ohtani, 1985; Tonks & Melosh, 1993). The nature of melt densification and thus the structures of silicate liquids above megabars would allow us to reveal the origins of the peculiar seismic properties of the dense silicate melts at the CMB and differentiation of primitive mantle during flow and subsequent mixing of mantle.

MgSiO_3 melt is among the primary components of dense melts and is key model systems for iron-free mafic mantle melts. Therefore, the structural adaptation in Mg silicate melts under compression is the key to solving negative buoyancy, potentially accounting for seismic observation of ULVZ. Despite the importance, their nature under the conditions of Earth's CMB remains unclear. Because oxygen anions contribute primarily to the volume of silicates, the overall densification of silicate melts is controlled by pressure-induced changes in the bonding configuration around oxygen. The presence of partial melts denser than the lower mantle silicate crystals in ULVZ near the bottom of the mantle has mainly been attributed to the potential partitioning of iron in the melts rather than in crystals, accounting for the observed density contrast (Caracas et al., 2019; Rost et al., 2005). In addition to such densification through iron enrichment, a dense packing of oxygen atoms, unique to compressed silicate melts above megabar pressures, may account for the presence of melts at the CMB (Lee et al., 2018; Lee et al., 2008).

Probing of bonding environments around oxygen is, therefore, crucial to understanding the nature of densification of silicate melts at the CMB. Despite its importance, little is known about the nature of oxygen-specific densification mechanisms under the conditions of Earth's interior as probing of the bonding transitions in MgSiO₃ glasses above megabar pressure conditions, particularly those around oxygen, is challenging. The challenge is mostly due to the structural disorder intrinsic to noncrystalline oxides and is partly due to the difficulty in collecting oxygen-specific structural information from mafic mantle melts.

In MgSiO₃ melt at 1 atm, polyhedral units (i.e., Si coordinated by multiple oxygen atoms in the first coordination shell, ⁴Si) are bridged through the ²O (bridging oxygen; BO) and nonbridging oxygen ¹O (NBO) (Allwardt & Stebbins, 2004; Gaudio et al., 2008; Lee et al., 2003; Lee et al., 2016). Below ~50 GPa, the structures of MgSiO₃ glasses have been extensively explored, revealing a decrease in the Si-O-Si angle and an increase in the Mg and Si coordination numbers upon compression (e.g., Fukui & Hiraoka, 2018; Kubicki et al., 1992; Lee et al., 2008; Moulton et al., 2016; Salmon et al., 2019; Wang et al., 2014 and references therein). Pioneering X-ray and Brillouin scattering studies of MgSiO₃ glasses above megabar pressure conditions (Kono et al., 2018; Murakami & Bass, 2011) revealed pressure-induced changes in the structure factors and acoustic wave velocities at ~90-140 GPa, suggesting the emergence of highly coordinated Si. While these structural changes in Si can result in structural evolution of the oxygen configuration, such as ³O (oxygen tricluster), together with the pressure-induced increase in BO at the expense of NBO (Lee et al., 2008), the nature of the oxygen bonding configurations in molten MgSiO₃ above megabar pressures remains to be revealed.

Synchrotron inelastic X-ray scattering (IXS) reveals otherwise hidden information on the direct bonding environments around target low-z elements at high pressure (e.g., Lee et al., 2014; Lee et al., 2018; Lin et al., 2007; Lin et al., 2011; Sternemann & Wilke, 2016 and references therein) (see S1). Indeed, oxygen K-edge IXS has been applied to explore the densification of MgSiO₃ glasses up to ~40 GPa (Lee et al., 2008). However, the pressure condition of the earlier study was not sufficient to fully account for the changes in melt properties at CMB (S1). While the inefficiency of IXS poses challenges for probing structures above 100 GPa, recent experimental advances in X-ray optics involving the post-collimation of scattered X-rays enabled collection of oxygen K-edge IXS signals for simple oxides, such as B₂O₃ and SiO₂ above megabar pressures (Chow et al., 2015; Lee et al., 2018; Lee et al., 2019). These studies offer opportunities to study transitions in oxygen environments in complex glasses. The changes in the electronic structures around oxygen through O K-edge IXS may provide a useful proxy for overall densification in Mg-bearing melts beyond 100 GPa. However, application of these IXS techniques to Mg-bearing silicate above megabar pressures has been largely limited. This is because of inefficiency in IXS measurement and an overlap among the spectroscopic features arising from the inherent disordered structure of depolymerized silicate glasses (S1). Here, we study the evolution of MgSiO₃ glasses and melts at high pressure up to 130 GPa using O K-edge IXS combined with *ab initio* molecular dynamics simulations, revealing the detailed bonding

nature of compressed oxygen atoms. The potential results unveil the structure, and thus a densification mechanism of dense melts, which are anticipated to comprise the ULVZ.

2. Materials and Methods

Glass synthesis and *in-situ* inelastic X-ray scattering. MgSiO₃ glass was synthesized by fusing MgO and SiO₂ mixture at 1650 °C for 30 min and quenching the melt by immersing the bottom of the Pt crucible into the water. Modified panoramic diamond anvil cell with diamond culet diameter of 150 μm was used for pressure generation. Sample was loaded into the Be gasket without pressure medium, resulting in a moderate pressure gradient. The O *K*-edge IXS spectra were collected at HPCAT beamline 16-ID-D of the Advanced Photon Source. The incident X-rays were monochromitized using a double-crystal Si(111), which was focused by a KB mirror pair, resulting in a beam size of a 8×5 μm² (FWHM) at the sample position. The IXS spectra were collected by scanning the X-ray energy relative to the analyzer energy of 9.9045 keV. Scattered photons were collected at a scattering angle of 25° with a poly-capillary post sample collimator, together with a single spherical Si(555) analyzer operating in a backscattering geometry (Chow et al., 2015; Lee et al., 2018). The O *K*-edge IXS spectra for MgSiO₃ glasses with varying pressures up to 130 GPa were collected with the step size and the energy loss (incident energy - analyzed energy) range of 0.5 eV and from 530 to 565 eV, respectively. Backgrounds were subtracted from the IXS spectra. Pressure conditions were estimated based on the Raman signal from the diamond culet (Akahama & Kawamura, 2007) (S2, Figs. S1 and S2). As there is a pressure gradient, the pressure at the center of the sample is reported in the current study (S2 for further details regarding the pressure estimation and the IXS setup).

***ab initio* molecular dynamics simulations and calculations of IXS spectra.** MgSiO₃ melt configurations with varying pressures and temperatures up to 131 GPa and 6000 K were prepared using *ab initio* molecular dynamics (MD) simulations within the Perdew-Burke-Ernzerhof (PBE) functional with the generalized gradient approximation (GGA) implemented in CASTEP (Clark et al., 2005). The ultrasoft pseudopotentials were used with a cutoff energy of 310 eV. The Γ -point Brillouin zone sampling was used for the self-consistent-field (SCF) calculation. The SCF convergence criterion for the total energy was set to 2×10⁻⁶ eV/atom. The MD calculations were performed using the *NVT* ensemble with the Nosé-Hoover-Langevin thermostat (Leimkuhler et al., 2009) and time-step was set to 1 fs. Cubic supercell containing 160 atoms (32 formula units) was used. The O *K*-edge IXS spectra were calculated by summing up the excitation features from 96 oxygen atoms from the snapshot of the melt configuration (Clark et al., 2005) (S3 for details).

3. Results & Discussion

Figure 1 shows the O *K*-edge IXS spectra for MgSiO₃ glass at varying pressures up to 130 GPa. In the current low-*q* setup, the O *K*-edge IXS feature mainly originates from the excitation of the oxygen 1s core electron into the empty σ^* antibonding 2*p* state (Lee et al., 2014 and references therein). The spectrum at 1 atm shows a feature centered at ~538-539 eV that stems from NBO (Mg-O-Si) and BO (Si-O-Si) (Lee et al., 2008). The main σ^*

feature shifts toward a higher energy loss region as pressure increases. Broad feature at ~544-545 eV emerges at ~30 GPa and persists until 130 GPa. The higher energy features are similar to the O *K*-edge features reported for the IXS spectra for SiO₂ glass at high pressure (Lee et al., 2019; Lin et al., 2007; Petitgirard et al., 2019): this feature has been attributed to the densification of the local network around oxygen in oxide glasses: suggested origins include an increase in the oxygen coordination number (i.e., formation of ¹²O at low pressure conditions and ¹³O at high pressure conditions) and associated changes in the medium-range length scale as well as topological evolution (e.g., increase in Si-O bond length and decrease in the Si-O-Si bond angle) (Lee et al., 2008). Recent *ab initio* simulations of crystalline MgSiO₃ indicated that the feature arises from diverse structural origins and is mainly correlated with a reduction in the O-O distance (Yi & Lee, 2016).

With a further increase in the pressure above ~90 GPa, an additional feature emerges at ~548 eV. The IXS feature shifts further toward a higher energy with substantial broadening. The prevalence of the high energy features suggests that the MgSiO₃ glass above megabar pressure may undergo additional densification that differs from that at lower pressures. To explore the atomistic origins of the high energy features, the O *K*-edge IXS features from the MgSiO₃ melt configurations up to ~131 GPa were calculated using *ab initio* simulations (see S3, S4, and S6). Figure 2 presents the pressure-induced changes in the calculated O *K*-edge IXS features (*left*) and the atomic structures (*right*) of MgSiO₃ melts. The experimental O *K*-edge IXS spectra of MgSiO₃ glasses (Figure 1) and those from previous theoretical studies on crystalline MgSiO₃ polymorphs (Yi & Lee, 2012; 2016) are also shown for comparison. Calculated spectra for crystalline MgSiO₃ show pressure-induced peak shifts with an increase in the intensity at ~543 eV upon phase transition (i.e., from corner-sharing Si tetrahedron to corner-sharing Si octahedron) (Yi & Lee, 2012; 2016), which is partly consistent with the changes observed in the glasses. The high energy features in the IXS spectra of MgSiO₃ glasses above 90 GPa, however, were not observed in the spectra of bridgmanite at 120 GPa, implying that the unique densified structures for MgSiO₃ glasses are not found in the crystalline analogs.

The *ab initio* MD simulations of the IXS features of MgSiO₃ liquids confirmed pressure-induced changes in the cation coordination numbers and Mg-O, Si-O, and O-O distances [Figure 2 (*right*); see S4 for additional information on the atomic structure of the melts]. First, the average coordination numbers of Mg (5.2 at ~1 atm) and Si (4.0 at ~1 atm) increase with increasing pressure: the average Mg and Si coordination numbers markedly increase to 6.7 and 4.5 at low pressures up to ~18 GPa, while they are 8 and 5.8, respectively, at ~131 GPa. The fraction of ^{15,6}Si increases to ~81% at ~51 GPa and ~94% at ~131 GPa, and the formation of ¹⁷Si (~6%) is also observed at ~131 GPa (see S4). The average Mg-O distance (2.249 Å at 1 atm) does not change significantly up to ~18 GPa (2.245 Å), but decreases to 2.202 Å at ~51 GPa, 2.162 Å at ~71 GPa, 2.122 Å at ~90 GPa, and to 2.044 Å at ~131 GPa. An increase in the Si-O distance from 1.683 Å (~1 atm) to 1.736 Å (~51 GPa) is observed. With a further increase in pressure, the Si-O distance slightly decreases to 1.733, 1.720, and 1.707 Å at ~71, 90, and 131 GPa, respectively. The

reduction in the average O-O distance is expected to play a major role in the overall densification of MgSiO₃ melts. Indeed, the average O-O distance significantly decreases upon compression (3.137 Å at ~1 atm, 2.920 Å at ~18 GPa, and ~2.457 Å at ~131 GPa).

The current *ab initio* simulations showed that densification of MgSiO₃ melts near the CMB is achieved *via* smooth and gradual reduction in the Mg-O and O-O distances and increase in ^{6,7}Si fraction (Figure S4), consistent with earlier *ab initio* results (Stixrude & Karki, 2005). These changes are illustrated in the Mg-O and O-O partial radial distribution functions (RDFs) of MgSiO₃ melts at ~131 GPa (S4; Figure S5). The overall changes in the average Mg-O, Si-O, and O-O distances for MgSiO₃ liquids are similar to those from earlier *ab initio* MD simulations of glassy analogs at 300 K (Ghosh et al., 2014) (S5; Figure S6), yet the mean distances were ~4-9% longer for the liquids due to thermal expansion. The estimated mean interatomic distances for MgSiO₃ bridgmanite at 3000 K based on the equation of state are also shown (Fiquet et al., 2000; Fiquet et al., 1998) (Figure S6). The difference in the Mg-O and O-O distances between MgSiO₃ crystals and melts decreases with increasing pressure, while the average Mg-O and O-O distances for melts are longer than those in crystals up to 130 GPa. Below 65 GPa, the average Si-O distance for melts is shorter than that of MgSiO₃ bridgmanite. However, the mean Si-O bond length in melts becomes longer than that in bridgmanite above 65 GPa because of the gradual increase in the average Si coordination number for MgSiO₃ melts over a broad pressure range.

The calculated O *K*-edge IXS spectra of MgSiO₃ melts present pressure-induced shifts in the main σ^* features. Features at ~544-545 and ~548 eV were also observed in the spectra at ~51 and ~131 GPa, respectively. Based on the similarities between the calculated O *K*-edge IXS spectra for MgSiO₃ melts and those for MgSiO₃ glasses [Figure 2 (*left*)], the high energy feature at ~548 eV for MgSiO₃ glasses above 90 GPa could be attributed to the gradual yet noticeable reductions in the Mg-O and O-O distances accompanied by the gradual increase in the Si coordination number. These highlight the densification path for noncrystalline MgSiO₃ above megabar pressure. As illustrated in S6 and Figure S7, the calculated partial electronic density of states (PDOS) for MgSiO₃ melts show an increase in the electronic hybridization between Mg and O at high pressure, confirming that the high energy feature arises from enhanced electronic interactions and the proximity between Mg-O. The *p-p* hybridization of the nearest neighboring oxygen atoms (O-O) also increases with pressure, contributing to the emergence of a feature near 548 eV (S6).

Note that the electronic bonding structures of MgSiO₃-bridgmanite showed that a delocalization of oxygen *d*-orbitals results in an observed broadening in the O *K*-edge IXS spectrum at 120 GPa, while oxygen *s*- and *p*-orbitals resulted in shifts with minor delocalization (Yi & Lee, 2016). In contrast, the electronic structures for the MgSiO₃ melts revealed the predominant contribution from oxygen *p*-orbitals above the Fermi level (S6; Figure S7), while the dispersion of the oxygen *d*-orbitals remained unchanged throughout the pressure range from 1 atm to ~131 GPa. These indicate inherent differences in the nature of the atomic arrangements in crystals and melts upon densification. In crystals,

the fixed crystallographic symmetry generates characteristic short- and long-range ordering in the atomic structures. These constraints in crystals result in severe electronic repulsion and subsequent delocalization of spatially dispersed electronic states (i.e., *d*-orbitals). However, disordered structures and the structural flexibility intrinsic to glasses and melts enable modification of the local atomic configuration to minimize the electronic interactions between dispersed electrons, thereby suppressing the dispersion of *d*-orbitals for noncrystalline MgSiO₃.

The simulations showed pressure-induced increases in the covalency of the Mg-O bonds in the melts, whereas those in the crystals remained largely unchanged (Yi & Lee, 2016) (S6; Figure S7). Recent IXS studies of SiO₂ glasses revealed the pressure-induced shift and broadening of the O *K*-edge features, similar to the MgSiO₃ glasses and melts (Lee et al., 2019; Lin et al., 2007; Petitgirard et al., 2019). The calculated electronic structures for SiO₂ crystals and glasses also present substantial contributions from the oxygen *d*-orbitals (Wu et al., 2012; Yi & Lee, 2012; 2016), in contrast to the MgSiO₃ melts, implying that an increase in the structural disorder upon the addition of Mg plays a major role in the electronic interactions for MgSiO₃ melts at high pressure. More in-depth discussion about the difference in IXS features for SiO₂ and MgSiO₃ glasses remains to be provided.

The detailed analysis of the O *K*-edge IXS features of MgSiO₃ glasses combined with the *ab initio* MD simulations revealed the densification of the depolymerized silicate magmas at the lowermost mantle. Recent IXS studies on simple oxide crystals and glasses have revealed that overall shifts in the O *K*-edge features, particularly shifts in the edge onset energy serve as structural proxies of the interatomic distances and bulk densities (Lee et al., 2018; Lee et al., 2019; Yi & Lee, 2012; 2016). For the MgSiO₃ glasses, Figure 3A presents the systematic shifts in the edge energy at the center of gravity (E_c) values of the MgSiO₃ crystals (Yi & Lee, 2012; 2016), glasses (Lee et al., 2008), and liquids with increasing density. As has been addressed in our studies of IXS spectra for diverse oxides at high pressure (Lee et al., 2018; Lee et al., 2019; Yi & Lee, 2016), the E_c of MgSiO₃ crystals and melts tend to increase linearly with bulk density. Furthermore, the E_c values for MgSiO₃ glasses estimated from the experimental IXS spectra (blue circles) form a trend line showing a rapid increase up to ~50 GPa and a rather gentle increase up to ~130 GPa, while there is a slight increase in the slope at ~90-100 GPa (Figs. 3B and 3C). We note that the change in slope may partly be due to the uncertainties in pressures and E_c (S2). The nonlinear trend in the E_c with varying pressure may result from the formation of ~548 eV feature as the emergence of the high energy feature at high pressure above 90 GPa may shift the E_c to even higher energy.

We note that progress has been made for the detailed analyses of the oxygen partial DOS under pressure [e.g., (Fukui et al., 2009; Lee et al., 2014; Yi & Lee, 2012; 2016), S1]: the changes in the electronic density of state patterns for MgSiO₃ glasses have diverse structural origins (i.e., all the changes in the short-to-medium range structures around oxygen upon compression) and often do not correspond to a unique structural response.

Particularly, an increase in the spectral intensities at ~ 548 eV was interpreted as an increase in the relative fraction of the densely connected oxygens with shortened Mg-O and O-O distances, consistent with the calculated changes in the RDF in Fig. S5. We note that the overall trends in the pressure-induced shifts in E_c for both crystalline and non-crystalline MgSiO_3 are similar. The pronounced similarity stems from the collective nature of the parameter, E_c , where the detailed atomic arrangements are averaged out. In detail, the structural evolutions of crystalline and non-crystalline are largely distinct as shown in the difference in the overall shape of the σ^* features (Figs. 1, 2, and Fig. S7 in S6). While a similar relationship between E_c and bulk density was demonstrated in other simple single component oxides at high pressure (Lee et al., 2019), the current results show that E_c can be used as a useful structural proxy for melt densification in more complex mantle melts.

4. Implication

While the process for creating denser melts and the pronounced negative buoyancy in the ULVZ remains a puzzle, the observed changes in atomic configurations and electronic structures, and structural disorder provide densification pathway to the deep mantle melts. Particularly, the detailed differences in the electronic bonding transition for crystalline and amorphous MgSiO_3 demonstrate the role of structural disorder and connectivity among $^{[n]}\text{Si}$ - and $^{[n]}\text{Mg}$ -polyhedra in overall densification (Figure 4): $^{[5,6,7]}\text{Si}$ polyhedra are inter-connected by bridging and edge-sharing oxygens and $^{[n]}\text{Mg}$ apparently forms a Mg-rich channel in MgSiO_3 liquids, resulting in a topologically disordered network characterized by heterogeneous and mesoscale distribution of $^{[5,6,7]}\text{Si}$ and $^{[n]}\text{Mg}$. In contrast, the distribution of $^{[6]}\text{Si}$ and $^{[n]}\text{Mg}$ is uniform in MgSiO_3 -bridgmanite, which partly accounts for the differences in the calculated O-O and Mg-O distance for the crystals and liquids. The current result suggests that the densification of deep melts can also be caused by structure (*via* configurational and topological compaction).

As also implied from the iron-rich crystalline phases that constitute a large low-shear-velocity province (LLSVP) in contact with the ULVZ (i.e., partitioning of iron into crystals), recent experiment revealed that partial melts in the ULVZ may be silica-rich (Andraut et al., 2014). Because MgO and SiO_2 are two main components of such melts, the structural changes and electronic density of states for simple MgSiO_3 glasses provide useful benchmarks to the densification in other multi-component silicate magmas above megabar pressures. While the actual melting of crystalline MgSiO_3 may not be feasible at ~ 130 GPa (Tateno et al., 2009), as dense partial melts near the CMB would have additional components, including FeO, melt densification near the CMB can be attributed to a preferential enrichment of iron in the melts (Rost et al., 2005); particularly, the density contrast in ULVZs at ~ 130 GPa can stem from both structural differences and preferential iron partitioning, while the latter may be mainly responsible for the density contrast. The current results with the IXS methods can also be applied to study the structures of more complex silicate melts under pressure conditions relevant to the CMB. The detailed bonding nature of such melts and the nature of densification may differ from those

observed for the pure MgSiO_3 glass. We postulate that heterogeneity in the melt composition and thus their somewhat different densification mechanisms partly account for seismic heterogeneities near the CMB (Shim & Catalli, 2009). Further experimental IXS studies on the MgSiO_3 liquids and beyond this simplified model system are necessary to detail the origin of the melt densifications at the CMB. The densification of MgSiO_3 melts, together with a potential change in melt densification with varying composition may contribute to the spatially *localized* gravitational stabilization of complex partial melts at the ULVZ.

5. Conclusion

The direct probing of electronic bonding transitions around oxygen in MgSiO_3 glasses above megabar pressure was performed *via* O K-edge IXS. Characteristic high energy features originate from the preferential contraction of Mg-O and O-O distances accompanied by the topological structural transformation of MgSiO_3 glasses. The results revealed that IXS features of MgSiO_3 glasses also correlate well with the bulk density. Analysis of the electronic density of states revealed that contributions from oxygen *d*-orbitals are suppressed in MgSiO_3 melts, while those are dominant in MgSiO_3 crystals, SiO_2 crystals and glasses. This difference arises from the flexible atomic arrangements in topologically disordered Mg networks in MgSiO_3 liquids. Together with melt densification near the CMB that has been attributed to a preferential enrichment of iron in the melts, the current results show a densification process based primarily on structural disorder in the melts toward the deep mantle.

Acknowledgments. This work was supported by National Research Foundation (NRF), Korea (2017R1A2A1A17069511) to S.K.L. HPCAT operations are supported by DOE-NNSA's Office of Experimental Sciences. Y.-H.K acknowledges the support by NRF-2017H1A2A1042446 through Global Ph.D. Fellowship. The Advanced Photon Source is a User Facility operated for the DOE Office of Science by Argonne National Laboratory under Contract No. DE-AC02-06CH11357. We thank two anonymous reviewers and the Editor Dr. Jacobsen for constructive comments and inputs, which greatly improved the manuscript's quality and clarity. All data used in this paper are provided and plotted in Figures 1-4, Figures S1-S7, and Table S1. IXS spectra for MgSiO_3 crystals in Figure 2 were retrieved from doi: <https://doi.org/10.1103/PhysRevB.94.094110>.

References

- Agee, C. B. (1998), Crystal-liquid density inversions in terrestrial and lunar magmas, *Physics of the Earth and Planetary Interiors*, 107(1), 63-74.
- Agee, C. B. & Walker, D. (1988), Static compression and olivine flotation in ultrabasic silicate liquid, *Journal of Geophysical Research: Solid Earth*, 93(B4), 3437-3449.
- Akahama, Y. & Kawamura, H. (2007), Diamond anvil Raman gauge in multimegabar pressure range, *High Pressure Research*, 27(4), 473-482.
- Allwardt, J. R. & Stebbins, J. F. (2004), Ca-Mg and K-Mg mixing around non-bridging O atoms in silicate glasses: An investigation using ^{17}O MAS and 3QMAS NMR, *American Mineralogist*, 89(5-6), 777-784.

- Andraut, D., Pesce, G., Bouhifd, M. A., Bolfan-Casanova, N., Hénot, J.-M., & Mezouar, M. (2014), Melting of subducted basalt at the core-mantle boundary, *Science*, 344(6186), 892-895.
- Caracas, R., Hirose, K., Nomura, R., & Ballmer, M. D. (2019), Melt-crystal density crossover in a deep magma ocean, *Earth and Planetary Science Letters*, 516, 202-211.
- Chow, P., Xiao, Y. M., Rod, E., Bai, L. G., Shen, G. Y., Sinogeikin, S., Gao, N., Ding, Y., & Mao, H.-K. (2015), Focusing polycapillary to reduce parasitic scattering for inelastic x-ray measurements at high pressure, *Review of Scientific Instruments*, 86(7), 072203.
- Clark, S. J., Segall, M. D., Pickard, C. J., Hasnip, P. J., Probert, M. J., Refson, K., & Payne, M. C. (2005), First principles methods using CASTEP, *Zeitschrift Fur Kristallographie*, 220(5-6), 567-570.
- Fiquet, G., Dewaele, A., Andraut, D., Kunz, M., & Le Bihan, T. (2000), Thermoelastic properties and crystal structure of MgSiO₃ perovskite at lower mantle pressure and temperature conditions, *Geophysical Research Letters*, 27(1), 21-24.
- Fiquet, G., Andraut, D., Dewaele, A., Charpin, T., Kunz, M., & Häusermann, D. (1998), P-V-T equation of state of MgSiO₃ perovskite, *Physics of the Earth and Planetary Interiors*, 105(1), 21-31.
- Fukui, H. & Hiraoka, N. (2018), Electronic and local atomistic structure of MgSiO₃ glass under pressure: A study of X-ray Raman scattering at the silicon and magnesium L-edges, *Physics and Chemistry of Minerals*, 45(2), 211-218.
- Fukui, H., Kanzaki, M., Hiraoka, N., & Cai, Y. Q. (2009), X-ray Raman scattering for structural investigation of silica/silicate minerals, *Physics and Chemistry of Minerals*, 36(3), 171-181.
- Gaudio, S. J., Sen, S., & Leshner, C. E. (2008), Pressure-induced structural changes and densification of vitreous MgSiO₃, *Geochimica et Cosmochimica Acta*, 72(4), 1222-1230.
- Ghosh, D. B., Karki, B. B., & Stixrude, L. (2014), First-principles molecular dynamics simulations of MgSiO₃ glass: Structure, density, and elasticity at high pressure, *American Mineralogist*, 99(7), 1304-1314.
- Kono, Y., Shibazaki, Y., Kenney-Benson, C., Wang, Y., & Shen, G. (2018), Pressure-induced structural change in MgSiO₃ glass at pressures near the Earth's core-mantle boundary, *Proceedings of the National Academy of Sciences*, 115(8), 1742-1747.
- Kubicki, J. D., Hemley, R. J., & Hofmeister, A. M. (1992), Raman and infrared study of pressure-induced structural changes in MgSiO₃, CaMgSi₂O₆, and CaSiO₃ glasses, *American Mineralogist*, 77(3-4), 258-269.
- Labrosse, S., Hernlund, J. W., & Coltice, N. (2007), A crystallizing dense magma ocean at the base of the Earth's mantle, *Nature*, 450, 866.
- Lee, S. K., Mysen, B. O., & Cody, G. D. (2003), Chemical order in mixed-cation silicate glasses and melts, *Physical Review B*, 68(21), 214206.
- Lee, S. K., Eng, P. J., & Mao, H. K. (2014), Probing of pressure-induced bonding transitions in crystalline and amorphous Earth materials: Insights from X-ray Raman scattering at high pressure, in *Spectroscopic Methods in Mineralogy and Materials Sciences*, edited by G. S. Henderson, D. R. Neuville & R. T. Downs, pp. 139-174.
- Lee, S. K., Kim, H.-I., Kim, E. J., Mun, K. Y., & Ryu, S. (2016), Extent of disorder in magnesium aluminosilicate glasses: Insights from ²⁷Al and ¹⁷O NMR, *The Journal of Physical Chemistry C*, 120(1), 737-749.
- Lee, S. K., Kim, Y.-H., Chow, P., Xiao, Y., Ji, C., & Shen, G. (2018), Amorphous boron oxide at megabar pressures via inelastic X-ray scattering, *Proceedings of the National Academy of Sciences*, 115(23), 5855-5860.

- Lee, S. K., Kim, Y.-H., Yi, Y. S., Chow, P., Xiao, Y., Ji, C., & Shen, G. (2019), Oxygen quadclusters in SiO₂ glass above megabar pressures up to 160 GPa revealed by x-ray Raman scattering, *Physical Review Letters*, accepted.
- Lee, S. K., et al. (2008), X-ray Raman scattering study of MgSiO₃ glass at high pressure: Implication for triclustered MgSiO₃ melt in Earth's mantle, *Proceedings of the National Academy of Sciences*, 105(23), 7925-7929.
- Leimkuhler, B., Noorizadeh, E., & Theil, F. (2009), A Gentle Stochastic Thermostat for Molecular Dynamics, *Journal of Statistical Physics*, 135(2), 261-277.
- Lin, J. F., et al. (2007), Electronic bonding transition in compressed SiO₂ glass, *Physical Review B*, 75, 012201.
- Lin, Y., Zhang, L., Mao, H.-k., Chow, P., Xiao, Y., Baldini, M., Shu, J., & Mao, W. L. (2011), Amorphous diamond: A high-pressure superhard carbon allotrope, *Physical Review Letters*, 107(17), 175504.
- Moulton, B. J. A., Henderson, G. S., Fukui, H., Hiraoka, N., de Ligny, D., Sonnevile, C., & Kanzaki, M. (2016), *In situ* structural changes of amorphous diopside (CaMgSi₂O₆) up to 20 GPa: A Raman and O K-edge X-ray Raman spectroscopic study, *Geochimica et Cosmochimica Acta*, 178, 41-61.
- Murakami, M., & Bass, J. D. (2011), Evidence of denser MgSiO₃ glass above 133 gigapascal (GPa) and implications for remnants of ultradense silicate melt from a deep magma ocean, *Proceedings of the National Academy of Sciences*, 108(42), 17286-17289.
- Ohtani, E. (1985), The primordial terrestrial magma ocean and its implication for stratification of the mantle, *Physics of the Earth and Planetary Interiors*, 38(1), 70-80.
- Petitgirard, S., Malfait, W. J., Sinmyo, R., Kuppenko, I., Hennet, L., Harries, D., Dane, T., Burghammer, M., & Rubie, D. C. (2015), Fate of MgSiO₃ melts at core-mantle boundary conditions, *Proceedings of the National Academy of Sciences*, 112(46), 14186-14190.
- Petitgirard, S., Sahle, C. J., Weis, C., Gilmore, K., Spiekermann, G., Tse, J. S., Wilke, M., Cavallari, C., Cerantola, V., & Sternemann, C. (2019), Magma properties at deep Earth's conditions from electronic structure of silica, *Geochemical Perspectives Letters*, 9, 32-37.
- Rost, S., Garnero, E. J., Williams, Q., & Manga, M. (2005), Seismological constraints on a possible plume root at the core-mantle boundary, *Nature*, 435, 666.
- Salmon, P. S., et al. (2019), Pressure induced structural transformations in amorphous MgSiO₃ and CaSiO₃, *Journal of Non-Crystalline Solids: X*, 3, 100024.
- Shim, S.-H. & Catalli, K. (2009), Compositional dependence of structural transition pressures in amorphous phases with mantle-related compositions, *Earth and Planetary Science Letters*, 283(1), 174-180.
- Sternemann, C. & Wilke, M. (2016), Spectroscopy of low and intermediate Z elements at extreme conditions: *In situ* studies of Earth materials at pressure and temperature via X-ray Raman scattering, *High Pressure Research*, 36(3), 275-292.
- Stixrude, L. & Karki, B. (2005), Structure and freezing of MgSiO₃ liquid in Earth's lower mantle, *Science*, 310(5746), 297-299.
- Tateno, S., Hirose, K., Sata, N., & Ohishi, Y. (2009), Determination of post-perovskite phase transition boundary up to 4400 K and implications for thermal structure in D'' layer, *Earth and Planetary Science Letters*, 277(1), 130-136.
- Tonks, W. B. & Melosh, H. J. (1993), Magma ocean formation due to giant impacts, *Journal of Geophysical Research: Planets*, 98(E3), 5319-5333.
- Wang, Y., Sakamaki, T., Skinner, L. B., Jing, Z., Yu, T., Kono, Y., Park, C., Shen, G., Rivers, M. L., & Sutton, S. R. (2014), Atomistic insight into viscosity and density of silicate melts under pressure, *Nature Communications*, 5, 3241.

Williams, Q. & Garnero, E. J. (1996), Seismic evidence for partial melt at the base of Earth's mantle, *Science*, 273(5281), 1528-1530.

Wu, M., Liang, Y., Jiang, J.-Z., & Tse, J. S. (2012), Structure and properties of dense silica glass, *Scientific Reports*, 2, 398.

Yi, Y. S. & Lee, S. K. (2012), Pressure-induced changes in local electronic structures of SiO₂ and MgSiO₃ polymorphs: Insights from ab initio calculations of O K-edge energy-loss near-edge structure spectroscopy, *American Mineralogist*, 97(5-6), 897-909.

Yi, Y. S. & Lee, S. K. (2016), Atomistic origins of pressure-induced changes in the O K-edge x-ray Raman scattering features of SiO₂ and MgSiO₃ polymorphs: Insights from *ab initio* calculations, *Physical Review B*, 94(9), 094110.

Accepted Article

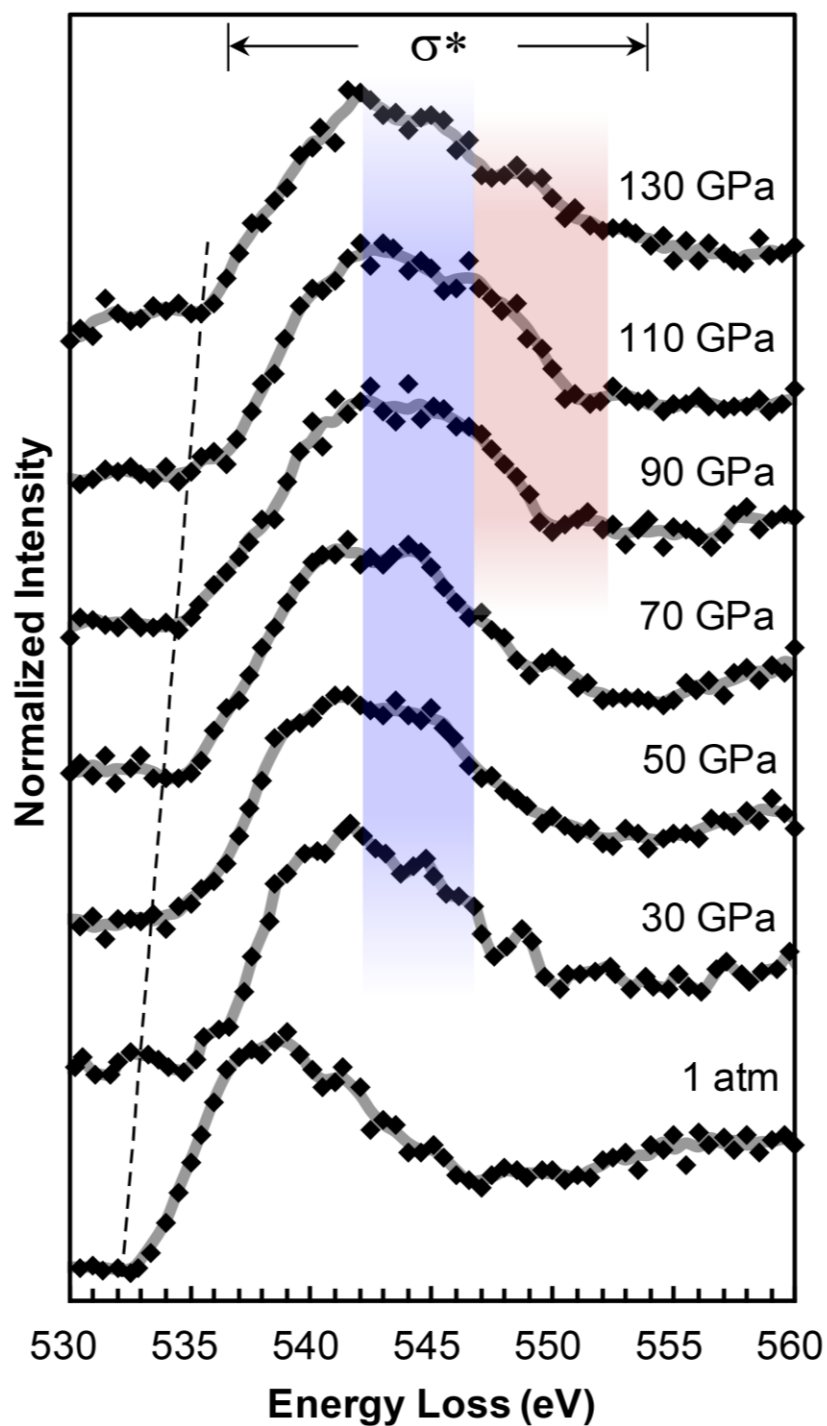


Fig. 1. Oxygen *K*-edge IXS spectra of MgSiO₃ glass with varying pressures up to ~130 GPa with respect to the energy loss (incident energy - elastic energy of 9.9045 keV). Spectrum at 30 GPa has been previously reported (Lee et al., 2008) but presented here for comparison.

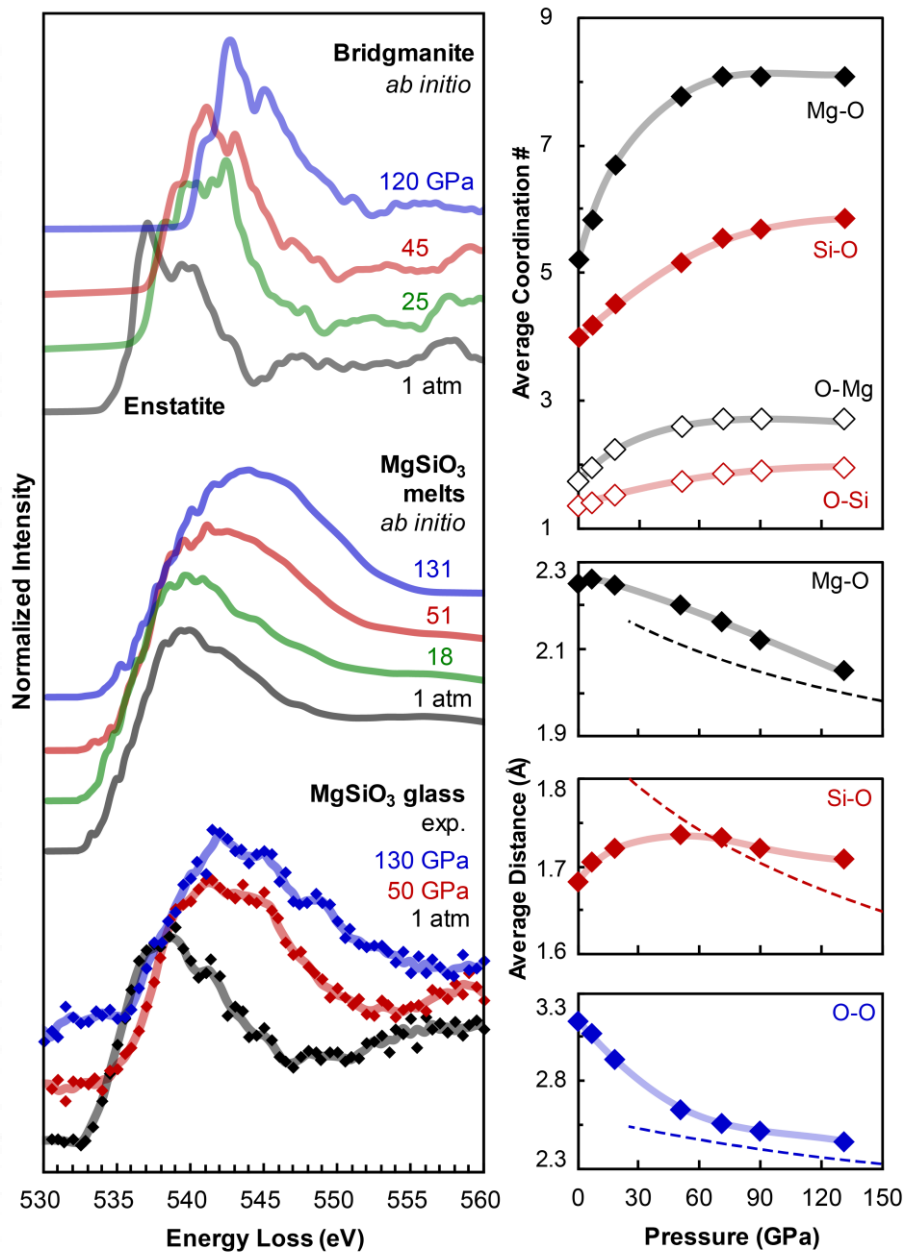


Fig. 2. (Left) Calculated oxygen *K*-edge IXS spectra for generated MgSiO₃ melts at 3000 K with varying pressures up to ~131 GPa. The experimental IXS spectra of MgSiO₃ glasses and previous theoretical IXS spectra for crystalline MgSiO₃ polymorphs (Yi & Lee, 2016) at similar pressure conditions are shown for comparison. (Right-top) Average coordination numbers of Mg-O (black), O-Mg (open black), Si-O (red), and O-Si (open red) for MgSiO₃ melts from *ab initio* molecular dynamics simulations as a function of pressures. Average coordination numbers were estimated from the first coordination shell of partial RDF for Mg-O and Si-O (see S4 and Figure S5). (Right-bottom) Changes in the average Mg-O, Si-O, and O-O distances for MgSiO₃ melts at 3000 K upon compression (filled diamonds). Dashed line indicates the average interatomic distances for bridgmanite estimated from the equation of state at 3000 K (Fiquet et al., 2000; Fiquet et al., 1998).

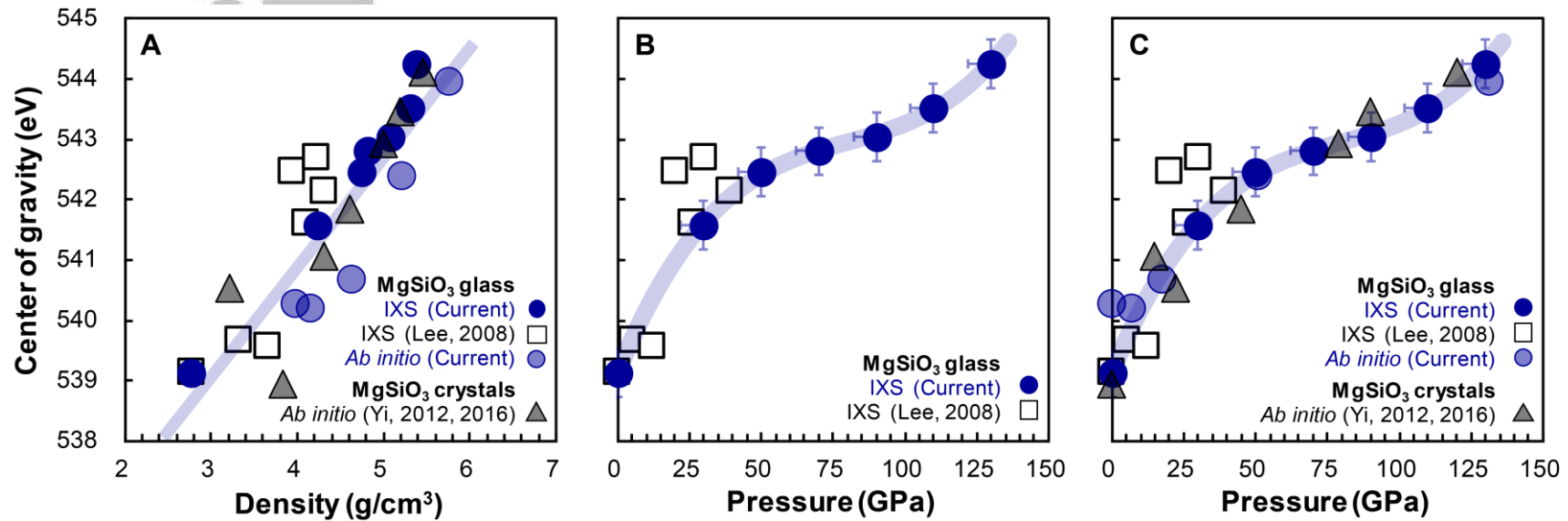


Fig. 3. (A) Relationship between the edge energy at the center of gravity (E_c) and density for MgSiO_3 crystals and glasses [$E_c(\text{eV}) \approx 1.83 \times \rho + 533.57$]. The densities of the MgSiO_3 glasses were from a recent experimental study (Petitgirard et al., 2015). (B) Pressure-induced changes in the E_c of the experimental O K -edge IXS features for MgSiO_3 glasses. (C) Pressure-induced changes in the E_c of the MgSiO_3 crystals [grey triangles (Yi & Lee, 2012; 2016)] and glasses [blue circles (current IXS experiment); open squares (Lee et al., 2008); pale blue circles (current *ab initio* calculations)]. Presented line shows the trend of the E_c from the experimental IXS spectra for MgSiO_3 glasses (blue circles). Uncertainties in the pressure and E_c are shown in the error bar (see S2).

Bridgmanite ~120 GPa

MgSiO₃ liquid ~130 GPa

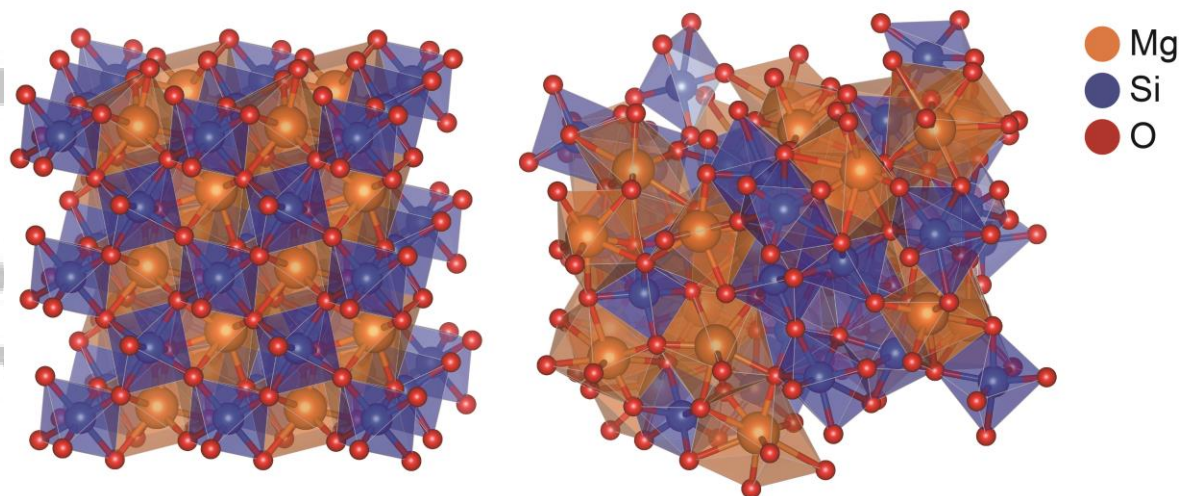


Fig. 4. Atomic structures of MgSiO₃ bridgmanite at 120 GPa (*left*) and a snapshot of configurations of MgSiO₃ liquids at 130 GPa *via ab initio* molecular dynamics simulations (*right*) as a model system for ULVZ melts. Light brown, red, and blue spheres refer to Mg, O, and Si, respectively. Mg and Si polyhedral units are shaded in pale brown and light blue, respectively.